

MicroCT-based imaging of microvasculature within the bone tissue

Version [v1.0](#) of this manuscript was submitted to [Small Methods](#) and is available as preprint at bioRxiv with the DOI [10.1101/2023.03.08.531678](https://doi.org/10.1101/2023.03.08.531678).

The version of the manuscript you see here ([permalink](#)) was automatically generated from [microct-ana-unibe-ch/microvasculature-manuscript@7b75b3e](#) on June 13, 2023. Changes to the submitted version are visualized [here on GitHub](#).

Authors

- **David Haberthür**  
[ID 0000-0003-3388-9187](#) ·  [habi](#) ·  @habi@mastodon.social
Institute of Anatomy, University of Bern, Baltzerstrasse 2, CH-3012 Bern, Switzerland
- **Oleksiy-Zakhar Khoma**  
[ID 0000-0002-1914-6873](#) ·  [ol-khoma](#)
Institute of Anatomy, University of Bern, Baltzerstrasse 2, CH-3012 Bern, Switzerland
- **Tim Hoessly**
Institute of Anatomy, University of Bern, Baltzerstrasse 2, CH-3012 Bern, Switzerland
- **Eugenio Zoni**
Department for BioMedical Research, Urology Research Laboratory, University of Bern, Bern, Switzerland; Department of Urology, Inselspital, Bern University Hospital, Bern, Switzerland
- **Marianna Kruithof-de Julio**  
[ID 0000-0002-6085-7706](#)
Department for BioMedical Research, Urology Research Laboratory, University of Bern, Bern, Switzerland; Department of Urology, Inselspital, Bern University Hospital, Bern, Switzerland; Department for BioMedical Research, Translation Organoid Research, University of Bern, Bern, Switzerland
- **Stewart D. Ryan**  
[ID 0000-0001-7016-771X](#)
U-Vet Hospital, University of Melbourne Veterinary School, Werribee, Australia
- **Myriam Grunewald**  
[ID 0000-0001-5394-9218](#)
Department of Developmental Biology and Cancer Research, Faculty of Medicine, The Hebrew University, Organoid Research Center, Hadassah University Hospital, Jerusalem, Israel
- **Benjamin Bellón**  
[ID 0000-0003-2297-9160](#)
Preclinical and Translational Research, Institut Straumann AG, Basel, Switzerland
- **Rebecca Sandgren**  
[ID 0000-0003-4473-4666](#)
Centre for Comparative Medicine, Medical Faculty, Lund University, Lund, Sweden

- **Benjamin E. Pippenger**

 [0000-0001-7990-5555](#)

Preclinical and Translational Research, Institut Straumann AG, Basel, Switzerland; Department of Periodontology, University of Bern, Bern, Switzerland

- **Dieter Bosshardt**

 [0000-0002-2132-6363](#)

Department of Periodontology, University of Bern, Bern, Switzerland

- **Valentin Djonov**

 [0000-0002-5062-1169](#)

Institute of Anatomy, University of Bern, Baltzerstrasse 2, CH-3012 Bern, Switzerland

- **Ruslan Hlushchuk** 

 [0000-0002-6722-8996](#)

Institute of Anatomy, University of Bern, Baltzerstrasse 2, CH-3012 Bern, Switzerland

⌚ — David Haberthür and Oleksiy-Zakhar Khoma contributed equally to this work.

✉ — Corresponding author: Ruslan Hlushchuk (ruslan.hlushchuk@unibe.ch, [+41 31 684 46 80](tel:+41316844680)).

Abstract

Angiogenesis is essential for skeletal development, bone healing and regeneration. Improved non-destructive, three-dimensional (3D) imaging of the vasculature within bone tissue would benefit a multitude of research areas, especially implantology and tissue engineering.

X-ray microtomography (microCT) is a well-suited non-destructive 3D imaging technique for bone morphology. For the detection of vessels, using contrast-enhanced microCT imaging is essential. Limited contrast between perfusion agents and mineralized bone has been the major drawback of this approach, making their distinct segmentation problematic. A decalcification step resolves this issue but inhibits simultaneous assessment of intracortical bone microstructure and vascular morphology. Moreover, the problem of contrasting becomes further compounded in samples with metal implants.

This study describes μ Angiofil-enhanced microCT-based visualization of vasculature within bone tissue in small and large animal models, with and without decalcification. We present simultaneous microvascular and bone imaging in murine tibia, murine bone metastatic model, pulp chamber, gingiva and periodontal ligaments. In a large animal model (minipig) we perform visualization and segmentation of different tissue types and vessels in the hemimandible containing metal implants.

Our manuscript introduces the first non-destructive approach for 3D imaging of the vasculature within soft and hard tissues in the vicinity of metal implants in a large animal model.

Introduction

Angiogenesis is an essential physiological vascularization process for skeletal development and growth as well as for bone healing and regeneration. This formation of new blood vessels from preexisting vessels is crucial for successful bone formation and repair [5]. In addition to carrying nutrients and growth factors, those newly formed blood vessels are a delivery route of stem cells and progenitor cells to the bone-defect site [6,7,8]. The structural nature of skeletal tissue makes three-dimensional (3D) imaging of its vasculature extremely difficult. Histology, a destructive and two-dimensional approach, still remains a gold standard for assessing vasculature in bones [9]. Classic soft tissue imaging techniques such as light sheet microscopy or confocal laser scanning microscopy face challenges in their application due to the encasement of blood vessels in calcified tissue [9]. Despite recent advancements in tissue clearing-based imaging methods for craniofacial bones in a mouse model [10,11], the application of such methods remains challenging. In the case of bone grafts, many of the synthetic ones fail to bridge critically sized defects due to their inability to promote vascularization [4,12]. In essence, simultaneous non-destructive 3D imaging of the vasculature within bone tissue and of the bone tissue itself, especially in the case of larger bone grafts, has been a challenge for decades [4,13]. Thus, many research areas benefit from an improved three-dimensional (3D) imaging of the vasculature within bone tissue: for example bone metastatic disease, bone biology, tissue engineering, implantology, reconstructive surgery and healing of both small and critical size bone defects with or without bone grafts.

In the last decades, X-ray micro-computed tomography (microCT) gained recognition as a non-destructive 3D imaging technique for bone morphology [14]. Due to the inherently low difference in X-ray absorption levels between vessels and different soft tissues it is not easily feasible to distinguish such structures within the bone. To unambiguously detect vasculature within bone it is thus necessary to instill the vessels with either a contrast agent or use a casting method to otherwise fill the blood vessels. Currently existing protocols for imaging the vasculature within the bone via a vascular replica, have drawbacks like showing disjoint vascular components or completely missing vascular segments [9,15]. It was also reported that the contrast difference between the perfusion agent to generate the replica of the vascular network and the mineralized bone make it problematic to perform a distinct segmentation of the bone tissue and the vasculature. This issue can be overcome by decalcifying samples prior to vascular imaging. Such a decalcification procedure makes simultaneous assessment of the intracortical bone microstructure and the vascular morphology impossible, though [9].

Intravascular contrast-agent-enhanced microCT has the potential to overcome these issues. It has become a method of choice for the evaluation of angiogenesis in bone tissue engineering and remodeling applications [2,4,16]. Barium sulfate and Microfil have been applied as the two most common contrast agents in studies on the vascularization of bone tissue. Only some selected studies [2] managed to show better perfusion and thus visualization when perfusing the vasculature with barium sulfate. Previous studies have reported disadvantages associated with barium sulfate suspensions, including higher viscosity, which can sometimes result in incomplete vascular filling and weak or inhomogeneous signal, particularly in higher resolution scans [2]. These issues may be attributed to particle aggregation, as indicated by various studies [17,18,19].

Although Microfil has probably been applied in a larger number of vasculature imaging studies than barium sulfate, Microfil was reported to have disadvantages like poor or incomplete filling of the vasculature [2,18,19] or vascular damage [20].

The problem of contrasting the vasculature becomes even further compounded in the presence of a metal implant. Even though such implants have revolutionized the treatment of patients with missing teeth or injured joints and bones [21,22], they are problematic for the tomographic image acquisition.

Due to their large X-ray absorption, metal implants produce beam hardening, partial volume and low signal artifacts in the resulting tomographic datasets [23]. Interactions occurring at the tissue-implant interface are widely believed to play a crucial role in the success of implant placement and healing [21,24]. High resolution imaging of the tissue-implant interface is complicated due to the aforementioned artifacts from the metal implants. Imaging with increased acceleration voltage and at small resolutions alleviates the imaging artifacts and makes microCT imaging the only available approach to non-destructively investigate the intact bone-implant interface in both 3D [21] and at in close proximity to the implant surface (i.e. closer than 200 μm).

Beyond studying the anatomy and physiology of angiogenesis and vasculature of the bone itself, the contribution of the vascular component in the healing process around bone-borne implants is also considered an area of study meriting further experimentation [4,25]. To date, only few studies tried to assess and visualize the vasculature surrounding implants using microCT imaging, for examples see [26], where Wang et al. assessed a region of 100 μm around the implant surface and [27], where Bhargava et al. present VascuViz, a pipeline for vascular systems biology and compare it to other vascular imaging workflows. Both these studies image the samples at approximately 7 μm voxel size, inhibiting the assessment of microvessels with a diameter of approximately 40 μm or less. To the best of our knowledge, no study has managed to resolve the microvascular component in a large animal model due to the technical limitations of the perfused contrast agent and the applied microCT imaging technique.

The present study introduces the polymer-based contrast agent μ Angiofil for high-resolution microCT-based visualization of microvasculature within bone tissue in small and large animal models, both with and without decalcification of the bone. Moreover, we show that μ Angiofil is suitable for simultaneous imaging and subsequent analysis of peri-implant hard and soft tissues as well as their vascularization in the vicinity of metal implants in a large animal model.

Materials, Methods and Results

Animals

In this study we used one transgenic VEGF male 21 months old mouse (see [28] for more details), five 6 weeks old CB17SCID male mice and two Göttingen minipigs. Animal procedures were performed in accordance with the applicable Swedish, Israeli or Swiss legislation on the protection of animals and were approved by the corresponding committees.

The murine experiment were approved by the local ethical committee of the Canton of Bern, Switzerland under the permit number BE 55/16. Minipig experiments were approved by the Malmö/Lund regional ethical committee, Sweden under license 5.8.18-15672/2019.

Contrast-enhanced microangioCT of mice using μAngiofil

The contrast agent μAngiofil (Fumedica AG, Switzerland) was prepared according to the manufacturer's recommendations. The perfusion of the mice was performed as previously described [29,30]. Briefly, heparinized animals were deeply anesthetized, the thorax and the peritoneal cavity were opened with scissors to expose the descending aorta. The exposed aorta was then cannulated in either antegrade (for the perfusion of the hind limbs) or retrograde direction (for the perfusion of the head and teeth) with a Venflon cannula (26 GA). Afterwards, the blood was flushed out with warm PBS solution. Several cuts of the liver edge allowed for effusion of the blood and buffer solution. Thereafter, the selected part of the body (hind limbs or head and teeth) was perfused with μAngiofil at 1–1.5 ml/min using a syringe pump. The perfusion lasted until the organ of interest appeared completely blue [30,31]. In bones, it is not possible to visually monitor this color change, thus perfusion of the neighboring soft tissues serves as an indirect marker of sufficient perfusion within the bone. To achieve correct perfusion of the vessels within the bone, we prolonged the perfusion time by instilling at least 2 ml of extra volume of contrast agent after all the superficial tissues of the extremity or head turned blue.. After harvesting, the samples were fixed by immersion in 4% paraformaldehyde (PFA) solution and then imaged using a SKYSCAN 1172 (Bruker microCT, Kontich, Belgium). The full collection of all relevant scanning and reconstruction parameters for each dataset shown in all figures is given in a table in the [Supplementary Materials](#). Very briefly, this scan was performed with an X-ray source acceleration voltage of 50 kV and an X-ray source current of 200 μA. The sample was rotated over totally 360° with one projection acquired at each 0.05° and 3 projections were averaged. This resulted in an isometric voxel size of 2.98 μm.

Figure 1 shows the bone microstructure and vascularization of a tibia of a 21-month-old VEGF transgenic male mouse. This visualization approach enabled a simultaneous display of bone, its vascularization, and their segmentation. As presented in our other study, we were able to quantitatively show that the age-related osteoporosis diminishes with improved vascularization [28].



Figure 1: microangiCT of proximal murine tibia of a 21-month-old VEGF transgenic male mouse. After perfusion with μ Angiofil the murine tibia was harvested, fixated in 4% PFA and imaged by microCT. Arrowheads mark microvessels within the tibia. The diameter of the tibia shaft is around 1 mm. On the right side of the image one can distinguish the bigger epiphyseal vessels. The bone tissue appears white at the plane of the virtual section through the microCT-dataset.

Decalcification of the μ Angiofil-perfused murine tibia

It is practically the standard in the field to decalcify the bone samples to enable the proper visualization and segmentation of vasculature within bone tissue [2,9]. We successfully established a bone-decalcifying protocol (for murine hind limb) with 10% ethylenediaminetetraacetic acid (EDTA) solution [32] by adapting previous work [15]. Decalcification of bone tissue does not negatively influence the bone structure itself, but reduces the X-ray absorption of bone tissue and thus makes it impossible to visualize simultaneously with the vasculature (Fig. 2).

<-! More about the method here ->

On the other hand, it enables tomographic imaging of the murine hind limb vasculature with less artifacts around the bone at lower acceleration voltages, which in most instances leads to shorter scanning times. These samples were imaged with a SKYSCAN 1172, all relevant parameters are given in the [Supplementary Materials](#). Very briefly, this scan was performed with an X-ray source acceleration voltage of 59 kV and an X-ray source current of 167 μ A. The X-rays were filtered by 0.2 mm of aluminum prior to incidence onto the sample. The sample was rotated over totally 180° with one projection acquired at each 0.1° and 2 projections were averaged. This resulted in an isometric voxel size of 3.19 μ m.

Furthermore, segmentation of the vasculature in the tomographic datasets becomes easier and a subsequent histological evaluation of the sample is facilitated [32].

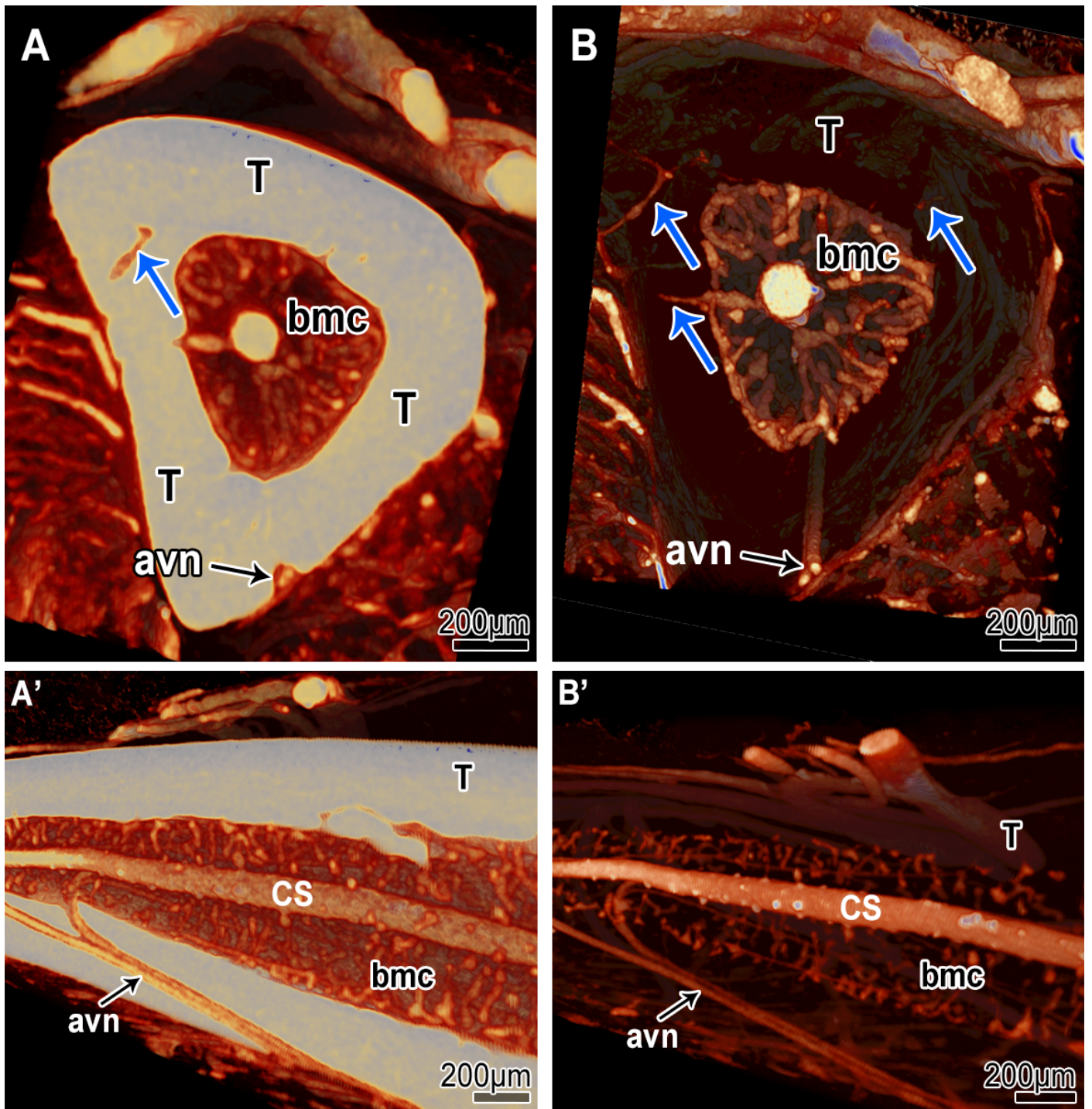


Figure 2: microangioCT-based visualization of the diaphysis of murine tibia before (A & A') and after decalcification with 10% EDTA (B & B'). In A and A' the tibia bone appears brighter and opaque due to higher X-ray absorption. In B and B' the tibia bone appears transparent due to its lowered X-ray absorption after decalcification. Due to the decalcification, connecting vessels between the periosteal vessels and the vessels of the bone marrow cavity (bmc) are more easily detectable (blue arrows in A vs. B). The visualization of the vessels within the medullar cavity (*central sinus* (CS)) is also improved. At the external surface of the tibia, supplying arteries are visible (*arteria et vena nutricia* (avn)).

Bone metastatic disease model, microangioCT

Assessment and 3D imaging of tumor vasculature is a challenging task, in almost every tumor model [33]. Due to the intraosseous location of tumor lesions, 3D microvascular imaging is even more challenging in a bone metastatic disease model. Since changes in bone and vasculature are believed to be of crucial importance for the progression of bone metastatic disease, simultaneous imaging of bone and vasculature is crucial. The desire to simultaneously assess existing bone defects makes the aforementioned decalcification procedure highly unfavorable.

To verify the suitability of our microangioCT approach for this kind of experimental imaging we used the following murine bone metastatic disease model. 50000 PC3-M-Pro4Luc2 dTomato cells were injected into the tibia of 6 weeks old CB17SCID male mice as previously described [34,35]. The X-ray assessment (25 kV, 6 sec, Faxitron Bi optics, Tucson, Arizona, US) was conducted at days 7, 14, 21 and 28 after implantation to monitor the progression of the lesions. Prior to terminal anesthesia and perfusion with μ Angiofil as described above, the hind limb of interest was X-rayed using Faxitron Bi optics as a standard follow-up in this model (see insert in Fig. 3, Panel A). The harvested and fixated murine hind limb was then imaged using a desktop microCT scanner SKYSCAN 1272 (Fig. 3), all relevant parameters are given in the [Supplementary Materials](#). Very briefly, this scan was performed with an X-ray source acceleration voltage of 60 kV and an X-ray source current of 166 μ A. The X-rays were filtered by 0.2 mm of aluminum prior to incidence onto the sample. The sample was rotated over totally 360° with one projection acquired at each 0.1° and 3 projections were averaged. This resulted in an isometric voxel size of 1.65 μ m.

The visualization (CTvox (v.3.3.1, microCT Bruker, Kontich, Belgium)) unambiguously displays intratumoral vasculature and extensive defects in mineralized bone tissue. Neighboring structures, such as the growth plate and the epiphysis or the menisci are also easily assessed (Fig. 3).

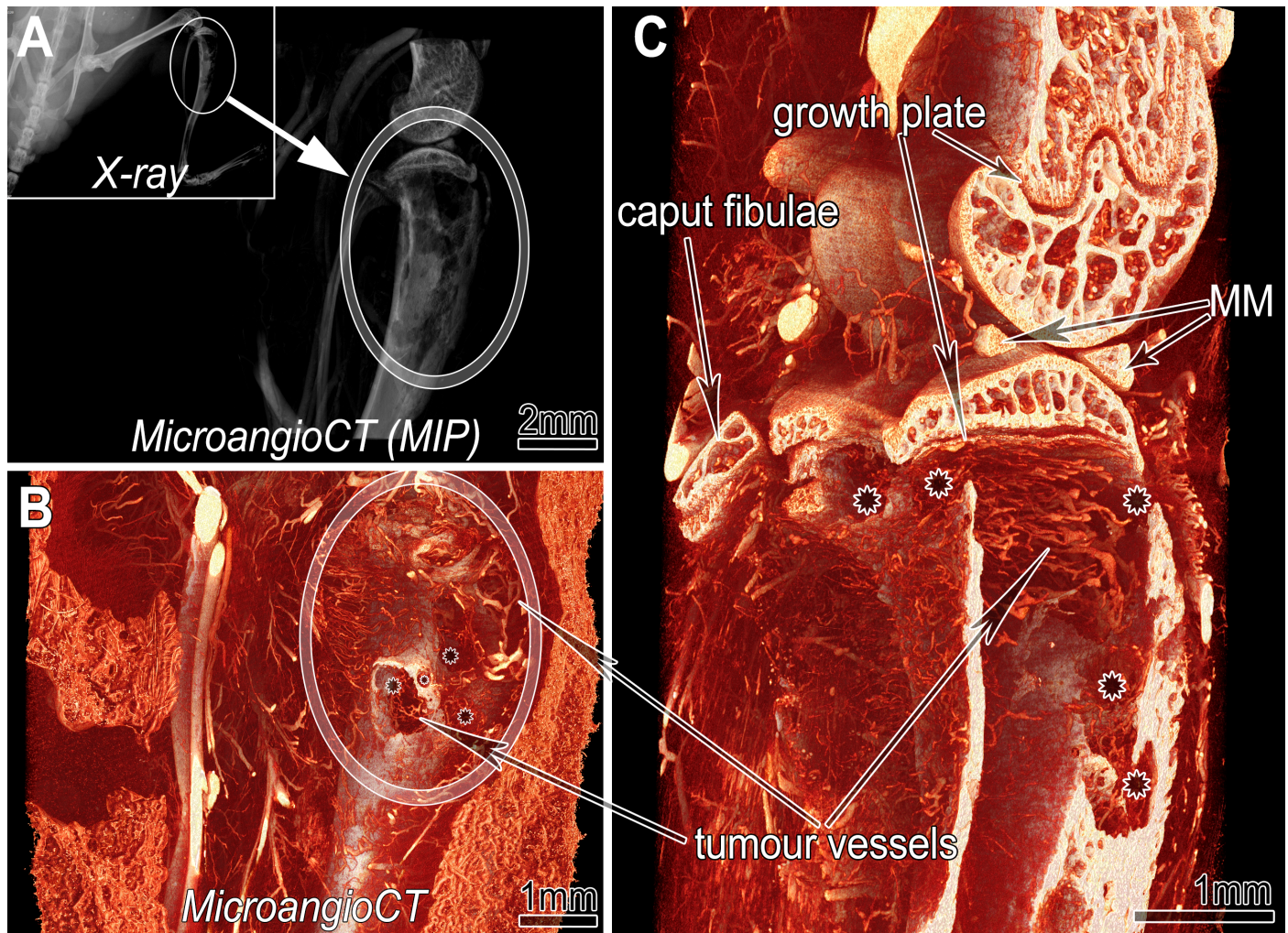


Figure 3: microangioCT of a xenograft tumor implanted into murine tibia. A: Maximum intensity projection (MIP) of the three-dimensional dataset of the investigated hind limb segment indicated in the inserted X-ray image of the mouse prior harvesting. Inset: X-ray image prior to terminal anesthesia. B: Virtual section through the microangioCT dataset visualizing remarkable defects represented as holes (asterisks in B and C) in the tibial bone at the tumor site (encircled). C: A more deeply positioned virtual section displaying the inner surface of the diseased tibia. Besides irregularly patterned tumor vessels (in B & C) further bony structures like growth plate or calcified parts of the medial meniscus (MM) are clearly distinguishable.

microangioCT of murine mandible and teeth

Murine mandibles and teeth are challenging for assessing the vasculature. This is due to the location of most of the vessels within the bone canals or in the proximity of the hard tissue. This consequently leads to the lack of larger bone-free volumes in which the vasculature is easily distinguishable. Nonetheless, with the improved perfusion protocol mentioned above and a well visualized difference between the X-ray absorption levels of μ Angiofil and mineralized bone tissue, we achieved appropriate imaging of such samples.

<-! More about the method here ->

The mouse teeth were imaged using a desktop microCT scanner SKYSCAN 1272 (Fig. 4), all relevant parameters are given in the [Supplementary Materials](#). Very briefly, this scan was performed with an X-ray source acceleration voltage of 80 kV.<-! AT WHICH CURRENT? "and an X-ray source current of XXX μ A."-> The X-rays were filtered by 0.2 mm of aluminum prior to incidence onto the sample. The sample was rotated over totally 360° with one projection acquired at each 0.1° and 4 projections were averaged. This resulted in an isometric voxel size of 1.0 μ m.

The microvasculature of murine mandible, periodontal ligament, and the teeth (even within their pulp chamber) can be clearly visualized without undergoing a decalcification procedure (Fig. 4).



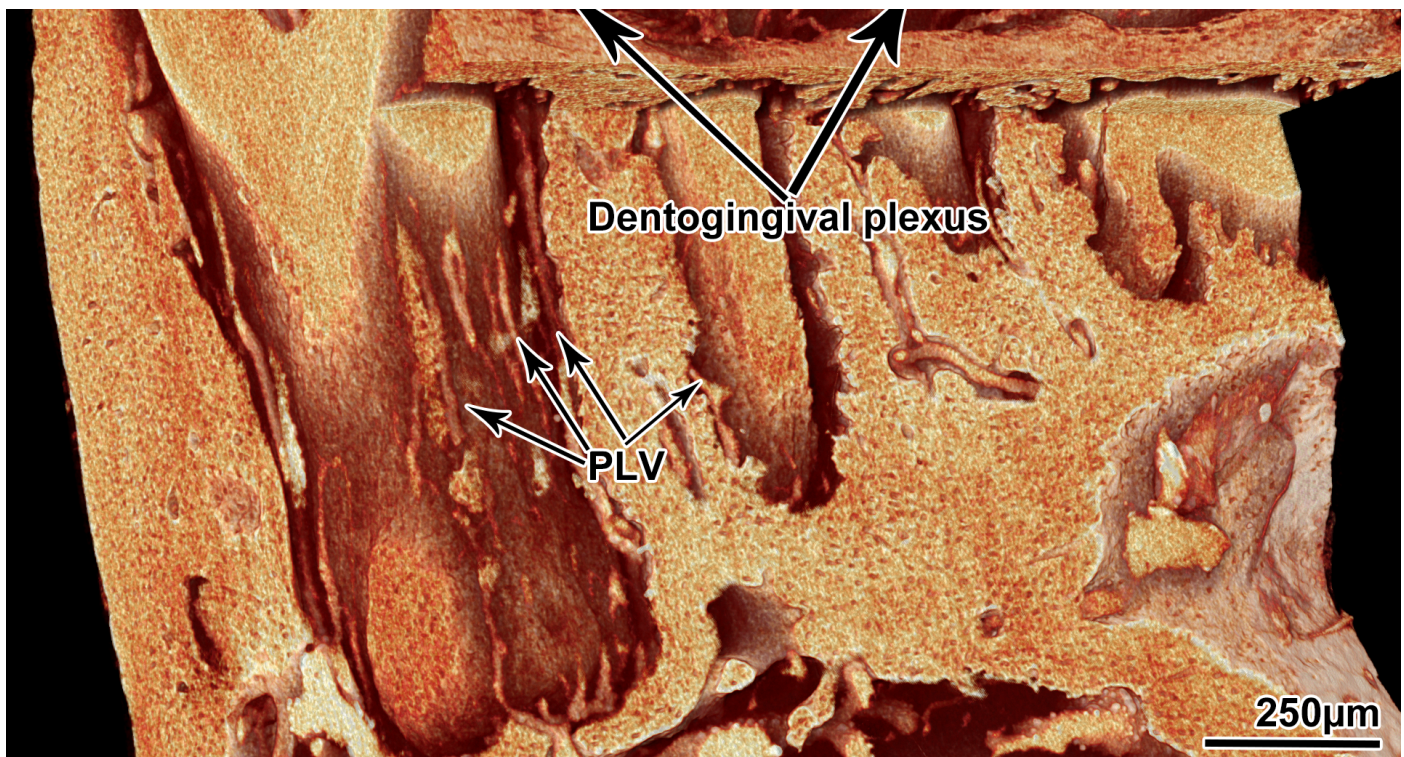


Figure 4: microangioCT of the vasculature of murine teeth. A: View onto a virtual section parallel to the crowns of the murine teeth: pulp chambers are visible, and the pulpal vessels are presented. The inset shows a full view of the tomographic dataset. B: Sagittal section through the mandible. The microvessels within the pulp cavities and root canals are distinguishable. C: Detailed view of the dentogingival plexus and periodontal ligament vessels (PLV).

microangioCT of mandible in a large animal model (Göttingen Minipig)

The Göttingen Minipig is widely recognized as a valuable animal model in preclinical dental and orofacial research, mainly because of its anatomical similarities to humans [36,37,38]. Its bone structure and bone remodeling processes closely resemble those of humans, further enhancing its suitability for such studies.

Göttingen minipigs (Ellegaard Göttingen Minipig, Dalmose, Denmark) were anesthetized intramuscularly (25–35 mg/kg, Dexdomitor; Orion Pharma Animal Health and 50–70 mg/kg, Zoletil 100 Vet, Virbac) and intravenously heparinized with 300 IE/kg (Heparin LEO, LEO Pharma). After heparin infusion, the pigs were euthanized with an intravenous dose (100 mg/kg) of pentobarbital (Euthanimal vet, VM Pharma). The external carotid artery was accessed by blunt dissection through tissue of the ventral neck and cannulated (BD Venflon, 17G). After washing out the blood with PBS, the corresponding head side was selectively perfused with μ Angiofil through the arterial tree. The perfusion was visually monitored equivalent to the previously described perfusion in mice. After polymerization of μ Angiofil (~30 min), the mandible was excised and fixated in 4% PFA solution. Mandibles were then later scanned using SKYSCAN 1273 (Fig. 5, panel A) or SKYSCAN 2214 (Fig. 5, panel B and C), all relevant parameters are given in the [Supplementary Materials](#). Very briefly, the scan for panel A was performed with an X-ray source acceleration voltage of 100 kV and an X-ray source current of 80 μ A. The X-rays were filtered by 1 mm of aluminum and 0.2 mm of copper prior to incidence onto the sample. The sample was rotated over totally 360° with one projection acquired at each 0.15° and 5 projections were averaged. This resulted in an isometric voxel size of 9 μ m. For the data shown in panels B and C, the scan was performed with an X-ray source acceleration voltage of 100 kV and an X-ray t current of 100 μ A. The X-rays were filtered by 1 mm of copper prior to incidence onto the sample. The sample was rotated over totally 360° with one projection acquired at each 0.18° and 4 projections were averaged. To horizontally overlapping projections were stitched to one to increase the imaged sample volume. This resulted in an isometric voxel size of 8 μ m. Data was visualized with CTvox (v.3.3.1).

Our approach provides excellent imaging of the whole mandible vasculature down to the vessels within the root canals and pulp chamber (Fig. 5).

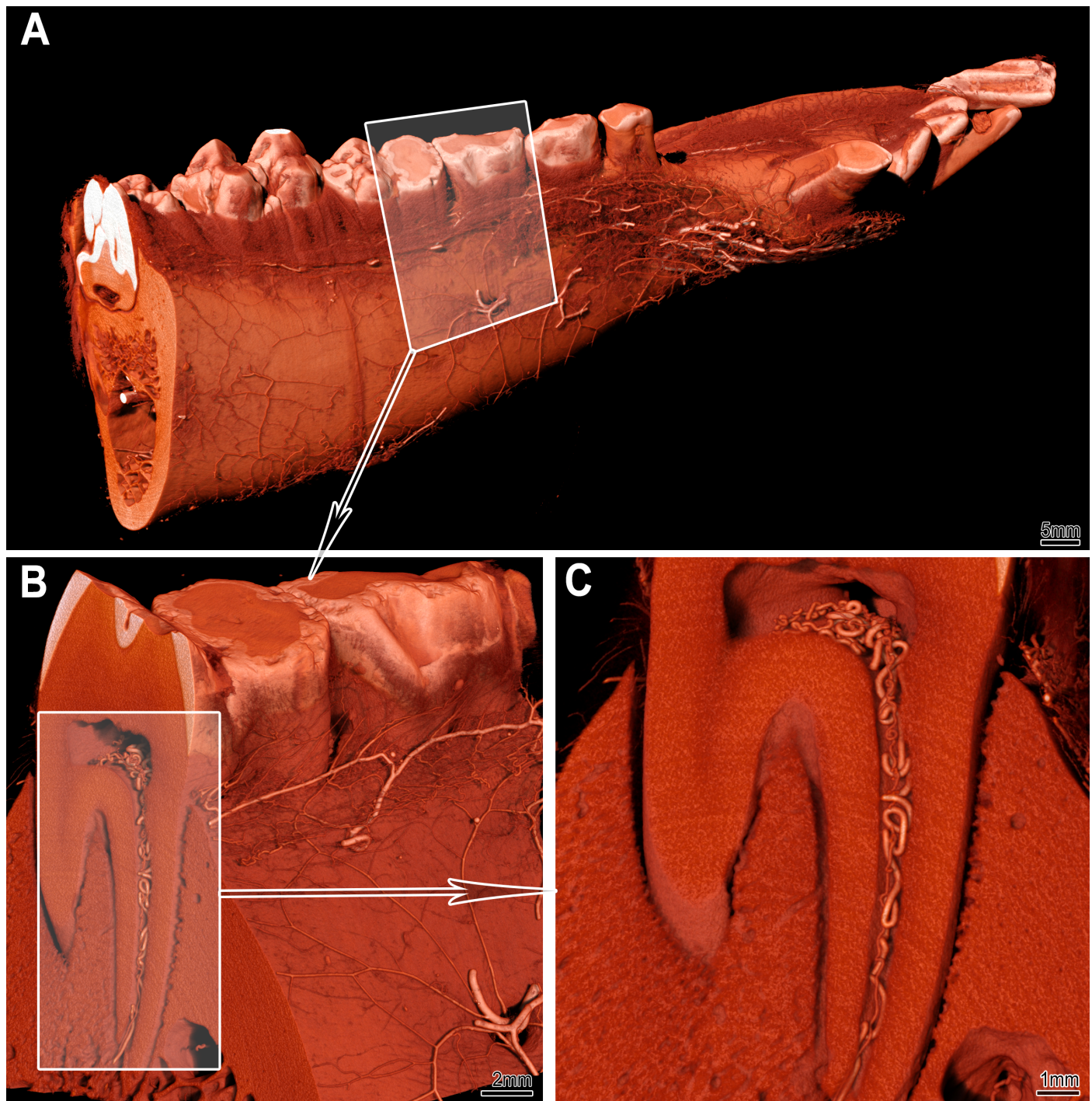


Figure 5: microangioCT of the minipig mandibula. Panel A displays the visualization of a right minipig hemimandible. The vasculature at the bone surface is clearly visible. The framed area in A marks the subvolume represented in panel B at higher magnification. Panel C displays the transverse section marked in panel B: the pulp chamber and root canal with the corresponding vessels are unambiguously visualized. Due to the voxel size of 8–9 μm , microvessels with diameter of 40 μm or less cannot be visualized in such large samples.

Osseointegration of implants is influenced by angiogenesis. As such, studying angiogenesis and, correspondingly the vascular supply of the peri-implant tissue in detail is important for dental research and many implantology studies. So far, the only reliable approach to assess the vascular supply remains histology, limited to single two-dimensional sections.

While microCT imaging allows for non-destructive, fully 3D imaging of dental research samples with implants, such imaging is a challenging task due to the presence of these metal parts with high

density and X-ray absorption within the samples. A decalcification step reduces the density of the sample but inevitably leads to the loss of information on the bone microstructure making the simultaneous assessment of the bone and vessels impossible [9]. For distinguishing the vasculature from both the metal implants and the mineralized bone tissue, the vasculature has to be instilled with a suitable contrast agent. The X-ray absorption characteristics of μ Angiofil make it possible to visualize and distinguish between soft tissue, bone tissue, contrast agent-filled vessels as well as metal implants according. We imaged an μ Angiofil-instilled minipig hemimandibula with a SKYSCAN 2214 (Fig. 6), all relevant parameters are given in the [Supplementary Materials](#). Very briefly, this scan was performed with an X-ray source acceleration voltage of 100 kV and an X-ray source current of 100 μ A. The X-rays were filtered by 1 mm of copper prior to incidence onto the sample. The sample was rotated over totally 360° with one projection acquired at each 0.18° and 4 projections were averaged. This resulted in an isometric voxel size of 8.0 μ m.

In the resulting tomographic datasets these regions of interest can easily be distinguished based on to their gray values ranges, as shown in Fig. 6, Panel C. Tomographic imaging of such samples and straightforward segmentation of features of interest without cumbersome post-processing (Fig. 6, Panel D) is enabled without requiring a decalcification step.

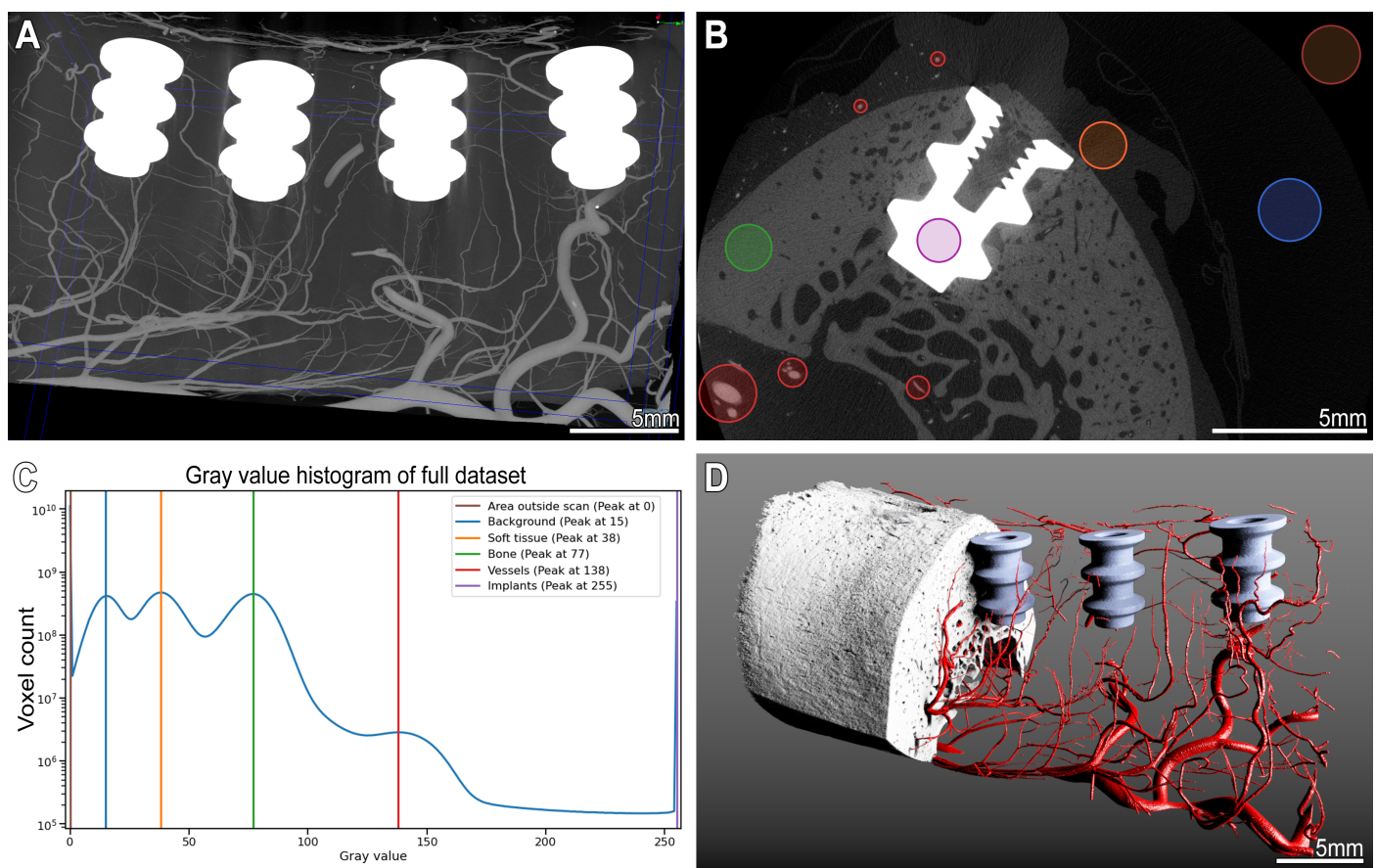


Figure 6: microangioCT of the peri-implant vasculature of a minipig mandibula. Panel A: Maximum intensity projection image of the minipig mandible dataset with 4 metal implants and μ Angiofil-perfused vessels. Panel B: virtual transversal section through the dataset showing an implant within the mandible. The colored circles mark structures with different gray values ranges. Corresponding peaks with color legend are marked on the histogram in panel C. Such differences in gray levels allow a straightforward segmentation of the structures of interest as displayed in the 3D visualization in panel D.

Discussion

Adequate vascularization is a prerequisite for successful bone formation and regeneration as well as osseointegration of biomaterials [1,39,40,41,42]. Without high-resolution imaging, the interplay between vasculature and bone tissue cannot be adequately studied, making it impossible to control these processes. Non-destructive microCT imaging is considered the only viable approach for 3D imaging of an intact bone-implant interface [21]. To properly distinguish the vasculature from other soft tissue structures, instillation of a contrast agent or producing an intravascular casting is necessary. Unfortunately, the microCT-based distinction of the vessels from other soft tissue structures is not possible without intravascular casting or instillation of contrast agents. Our hereby presented method of imaging the microvasculature within bones based on instillation with μ Angiofil overcomes several drawbacks of previously described methods (for details, see [Introduction](#) for a thorough explanation) and is suitable for the visualization of the microvasculature within bone tissue with or without decalcification (Fig. 2). The developed decalcifying protocols enable correlative imaging of the same sample with preserved intravascular contrast agent with subsequent classical histological evaluation [32]. Distinct differences in the X-ray attenuation of μ Angiofil and the bone tissue allow for assessing vascularization and bone growth without the need for repeated tomographic scans (before and after decalcification) and subsequent registration. This saves machine and labor time and does not damage the sample composition.

The microangioCT approach we present here can be used for simultaneous visualization of the hard (and eventually soft) tissues and their vascularization in small and large animal models. One of the noteworthy possible applications of this approach is simultaneous visualization of the bone microarchitecture and microvasculature of bone metastases in a murine xenograft tumor model (Fig. 3). Especially for studying bone metastatic models it is crucial to find a method that allows for the correct assessment of the microvasculature without decalcifying the sample. Such a decalcification would hinder the thorough assessment of pathological processes in bone tissue. These pathological processes can lead to so-called skeletal-related-events, which are associated with shortened survival and deterioration of quality of life [43], and should therefore be avoided. Our method allows to study the response to specific treatments, including bone-targeted and antiangiogenic therapies. These can be assessed within the same sample and in 3D, and be followed up with a histological examination if desired [44]. The presented method could offer additional insights into the interplay between angiogenesis and bone growth, bone lysis, and bone turnover, which have not been fully elucidated yet. The results will be crucial for selecting potential drug candidates and proper treatment decision and efficacy prediction.

In dental research, preclinical models can be divided into small and large animals. Small animal models, particularly mice and rats, are highly popular, due to their practical size and cost-effectiveness. The microCT scan of correspondingly small samples perfused with μ Angiofil can be performed with a voxel size around 1 μ m, providing excellent detail resolution (Fig. 4).

Nonetheless, the small size of hemimandible samples and availability of the transgenic lines would allow for a recently published imaging approach [21] in the murine models. This tissue-clearing-based approach could be a viable option for the visualization of the peri-implant tissues and vasculature in small animal models. There are limitations of such a tissue-clearing-based imaging approach, though. Namely i) differential shrinkage among soft and hard tissues, leading to anisotropic distortion in samples where both tissue types (plus eventual metal implant) are present; ii) limited depth (around 800 μ m in a mouse model [21]) due to the challenges of achieving complete transparency of bone tissue. Large anisotropic distortion of the sample may lead to the alteration of the common site of interest, namely the implant-tissue interface. The limitation of the maximal achievable visible depth makes such an approach impracticable for usage in large animal models.

Our presented microangioCT approach does not have such limitations and can be easily applied for visualization of hemimandible and its vascularization in a large animal model like Göttingen minipig (Fig. 5). μ Angiofil has noticeably different attenuation than mineralized bone and allows for distinct distinction, segmentation and visualization of soft tissue, bone tissue, vessels filled with the contrast agent as well as metal implants according to their gray values in the histogram (Fig. 6).

To the best of our knowledge, ours is the first study demonstrating non-destructive 3D imaging of the microvasculature of bone in the proximity of metal objects/implants in a large animal model.

Limitations of our approach

The most significant limitation of the suggested approach is the general limitation of microCT imaging, namely, the correlation between the resolution and the sample size. If the sample is only a few millimeters in diameter, the voxel sizes in the range of 1 μ m enable visualization of the microvasculature down to the capillary bed [29,30,31,32]. In case of large samples, like minipig hemimandible, the achievable voxel size is approximately 10 times larger ($\geq 8 \mu\text{m}$). In such samples the finest microvessels with diameter under 40 μm thus cannot be accurately visualized (see Fig. 5 & 6).

Nonetheless, the presented approach is, according to our knowledge, the best what can be achieved with the modern microCT scanners and is a big step forward for qualitative and quantitative imaging in tissue engineering and implantology research as well as many other related research fields.

Author Contributions

[Contributor Roles Taxonomy](#), as defined by the [National Information Standards Organization](#).

Author	Contributions
David Haberthür	Data curation; Formal analysis; Investigation; Project administration; Software; Validation; Visualization; Writing – original draft; Writing – review & editing
Oleksiy-Zakhar Khoma	Data curation; Formal analysis; Investigation; Project administration; Software; Validation; Visualization; Writing – original draft; Writing – review & editing
Tim Hoessly	Data curation; Investigation; Writing – review & editing
Eugenio Zoni	Resources; Writing – review & editing
Marianna Kruithof-de Julio	Resources; Writing – review & editing
Stewart D. Ryan	Resources; Writing – review & editing
Myriam Grunewald	Resources; Writing – review & editing
Benjamin Bellón	Methodology; Writing – review & editing
Rebecca Sandgren	Resources; Writing – review & editing
Benjamin E. Pippenger	Methodology; Writing – review & editing
Dieter Bosshardt	Methodology; Writing – review & editing
Valentin Djonov	Conceptualization; Funding acquisition; Supervision; Writing – review & editing
Ruslan Hlushchuk	Conceptualization; Funding acquisition; Investigation; Methodology; Project administration; Supervision; Validation; Writing – original draft; Writing – review & editing

Conflicts of interest

Author	Conflict
Benjamin Bellón	Employed by a company producing dental implants
Benjamin E. Pippenger	Employed by a company producing dental implants

Acknowledgments

We are grateful to the [Microscopy Imaging Center](#) of the University of Bern for infrastructural support. We thank the `manubot` project [45] for helping us write this manuscript collaboratively.

Supplementary Materials

Log files of all the tomographic scans performed for this study

The CSV file [ScanningDetails.csv](#) gives a tabular overview of all the (relevant) parameters of all the scans we performed. This file was generated with a [data processing notebook](#) and contains information read from *all* the log files of *all* the scans we performed. A copy of each log file is available [online](#).

References

1. **Long-term cell-mediated protein release from calcium phosphate ceramics**
Ellen Wernike, Willy Hofstetter, Yuelian Liu, Gang Wu, Hans-Jörg Sebald, Daniel Wismeijer, Ernst B Hunziker, Klaus-Arno Siebenrock, Frank M Klenke
Journal of Biomedical Materials Research Part A (2009) <https://doi.org/bmqbc8>
DOI: [10.1002/jbm.a.32411](https://doi.org/10.1002/jbm.a.32411) · PMID: [19195029](#)
2. **Structure and quantification of microvascularisation within mouse long bones: What and how should we measure?**
Bernard Roche, Valentin David, Arnaud Vanden-Bossche, Françoise Peyrin, Luc Malaval, Laurence Vico, Marie-Hélène Lafage-Proust
Bone (2012-01) <https://doi.org/bpvpm>
DOI: [10.1016/j.bone.2011.09.051](https://doi.org/10.1016/j.bone.2011.09.051) · PMID: [22019874](#)
3. **Bone Vascularization in Normal and Disease Conditions**
Christian Carulli, Massimo Innocenti, Maria Luisa Brandi
Frontiers in Endocrinology (2013) <https://doi.org/gr738c>
DOI: [10.3389/fendo.2013.00106](https://doi.org/10.3389/fendo.2013.00106) · PMID: [23986744](#) · PMCID: [PMC3752619](#)
4. **State-of-the-art techniques for imaging the vascular microenvironment in craniofacial bone tissue engineering applications**
Yunke Ren, Janaka Senarathna, Warren L Grayson, Arvind P Pathak
American Journal of Physiology-Cell Physiology (2022-11-01) <https://doi.org/gr7378>
DOI: [10.1152/ajpcell.00195.2022](https://doi.org/10.1152/ajpcell.00195.2022) · PMID: [36189973](#) · PMCID: [PMC9829486](#)
5. **The role of vasculature in bone development, regeneration and proper systemic functioning**
Joanna Filipowska, Krzysztof A Tomaszewski, Łukasz Niedźwiedzki, Jerzy A Walocha, Tadeusz Niedźwiedzki
Angiogenesis (2017-02-13) <https://doi.org/gbn8bj>
DOI: [10.1007/s10456-017-9541-1](https://doi.org/10.1007/s10456-017-9541-1) · PMID: [28194536](#) · PMCID: [PMC5511612](#)
6. **Dual release of growth factor from nanocomposite fibrous scaffold promotes vascularisation and bone regeneration in rat critical sized calvarial defect**
Shruthy Kuttappan, Dennis Mathew, Jun-ichiro Jo, Ryusuke Tanaka, Deepthy Menon, Takuya Ishimoto, Takayoshi Nakano, Shantikumar V Nair, Manitha B Nair, Yasuhiko Tabata
Acta Biomaterialia (2018-09) <https://doi.org/gr737v>
DOI: [10.1016/j.actbio.2018.07.050](https://doi.org/10.1016/j.actbio.2018.07.050) · PMID: [30067947](#)
7. **Angiogenesis involvement by octacalcium phosphate-gelatin composite-driven bone regeneration in rat calvaria critical-sized defect**
Tsuyoshi Kurobane, Yukari Shiwaku, Takahisa Anada, Ryo Hamai, Kaori Tsuchiya, Kazuyoshi Baba, Masahiro Iikubo, Tetsu Takahashi, Osamu Suzuki
Acta Biomaterialia (2019-04) <https://doi.org/gr737w>
DOI: [10.1016/j.actbio.2019.02.021](https://doi.org/10.1016/j.actbio.2019.02.021) · PMID: [30776505](#)
8. **It Takes Two to Tango: Coupling of Angiogenesis and Osteogenesis for Bone Regeneration**
Andrea Grosso, Maximilian G Burger, Alexander Lunger, Dirk J Schaefer, Andrea Banfi, Nunzia Di Maggio
Frontiers in Bioengineering and Biotechnology (2017-11-03) <https://doi.org/gckgs4>
DOI: [10.3389/fbioe.2017.00068](https://doi.org/10.3389/fbioe.2017.00068) · PMID: [29164110](#) · PMCID: [PMC5675838](#)

9. **Simultaneous visualisation of calcified bone microstructure and intracortical vasculature using synchrotron X-ray phase contrast-enhanced tomography**
Juan A Núñez, Alice Goring, Eric Hesse, Philipp J Thurner, Philipp Schneider, Claire E Clarkin
Scientific Reports (2017-10-16) <https://doi.org/gcfxxb>
DOI: [10.1038/s41598-017-13632-5](https://doi.org/10.1038/s41598-017-13632-5) · PMID: [29038597](#) · PMCID: [PMC5643345](#)
10. **Quantitative 3D imaging of the cranial microvascular environment at single-cell resolution**
Alexandra N Rindone, Xiaonan Liu, Stephanie Farhat, Alexander Perdomo-Pantoja, Timothy F Witham, Daniel L Coutu, Mei Wan, Warren L Grayson
Nature Communications (2021-10-28) <https://doi.org/gr7373>
DOI: [10.1038/s41467-021-26455-w](https://doi.org/10.1038/s41467-021-26455-w) · PMID: [34711819](#) · PMCID: [PMC8553857](#)
11. **Investigation of Postnatal Craniofacial Bone Development with Tissue Clearing-Based Three-Dimensional Imaging**
Wenjing Luo, Yating Yi, Dian Jing, Shiwen Zhang, Yi Men, Woo-Ping Ge, Hu Zhao
Stem Cells and Development (2019-10-01) <https://doi.org/gr7375>
DOI: [10.1089/scd.2019.0104](https://doi.org/10.1089/scd.2019.0104) · PMID: [31392933](#) · PMCID: [PMC6767869](#)
12. **Vascularization Strategies for Tissue Engineering**
Michael Lovett, Kyongbum Lee, Aurelie Edwards, David L Kaplan
Tissue Engineering Part B: Reviews (2009-09) <https://doi.org/fsjhcx>
DOI: [10.1089/ten.teb.2009.0085](https://doi.org/10.1089/ten.teb.2009.0085) · PMID: [19496677](#) · PMCID: [PMC2817665](#)
13. **Vascularization in Bone Tissue Engineering Constructs**
Ángel E Mercado-Pagán, Alexander M Stahl, Yaser Shanjani, Yunzhi Yang
Annals of Biomedical Engineering (2015-01-24) <https://doi.org/f66z3g>
DOI: [10.1007/s10439-015-1253-3](https://doi.org/10.1007/s10439-015-1253-3) · PMID: [25616591](#) · PMCID: [PMC4979539](#)
14. **Modalities for Visualization of Cortical Bone Remodeling: The Past, Present, and Future**
Kimberly D Harrison, David ML Cooper
Frontiers in Endocrinology (2015-08-11) <https://doi.org/gr738d>
DOI: [10.3389/fendo.2015.00122](https://doi.org/10.3389/fendo.2015.00122) · PMID: [26322017](#) · PMCID: [PMC4531299](#)
15. **Simultaneous 3D visualization and quantification of murine bone and bone vasculature using micro-computed tomography and vascular replica**
Philipp Schneider, Thomas Krucker, Eric Meyer, Alexandra Ullmann-Schuler, Bruno Weber, Marco Stampanoni, Ralph Müller
Microscopy Research and Technique (2009-09) <https://doi.org/ftspdd>
DOI: [10.1002/jemt.20720](https://doi.org/10.1002/jemt.20720) · PMID: [19360841](#)
16. **Microcomputed Tomography Characterization of Neovascularization in Bone Tissue Engineering Applications**
Simon Young, James D Kretlow, Charles Nguyen, Alex G Bashoura, LScott Baggett, John A Jansen, Mark Wong, Antonios G Mikos
Tissue Engineering Part B: Reviews (2008-09) <https://doi.org/b5snxg>
DOI: [10.1089/ten.teb.2008.0153](https://doi.org/10.1089/ten.teb.2008.0153) · PMID: [18657028](#) · PMCID: [PMC2761680](#)
17. **New polyurethane-based material for vascular corrosion casting with improved physical and imaging characteristics**
Thomas Krucker, Axel Lang, Eric P Meyer
Microscopy Research and Technique (2006) <https://doi.org/d6dwtd>
DOI: [10.1002/jemt.20263](https://doi.org/10.1002/jemt.20263) · PMID: [16456839](#)

18. **Novel methods for microCT-based analyses of vasculature in the renal cortex reveal a loss of perfusable arterioles and glomeruli in eNOS-/ mice**
Daniel S Perrien, Mohamed A Saleh, Keiko Takahashi, Meena S Madhur, David G Harrison, Raymond C Harris, Takamune Takahashi
BMC Nephrology (2016-03-02) <https://doi.org/gr738b>
DOI: [10.1186/s12882-016-0235-5](https://doi.org/10.1186/s12882-016-0235-5) · PMID: [26936597](https://pubmed.ncbi.nlm.nih.gov/26936597/) · PMCID: [PMC4776352](https://pubmed.ncbi.nlm.nih.gov/PMC4776352/)
19. **A Review of Ex Vivo X-ray Microfocus Computed Tomography-Based Characterization of the Cardiovascular System**
Lisa Leyssens, Camille Pestiaux, Greet Kerckhofs
International Journal of Molecular Sciences (2021-03-23) <https://doi.org/gr738g>
DOI: [10.3390/ijms22063263](https://doi.org/10.3390/ijms22063263) · PMID: [33806852](https://pubmed.ncbi.nlm.nih.gov/33806852/) · PMCID: [PMC8004599](https://pubmed.ncbi.nlm.nih.gov/PMC8004599/)
20. **Development of barium-based low viscosity contrast agents for micro CT vascular casting: Application to 3D visualization of the adult mouse cerebrovasculature**
Sung-Ha Hong, Alexander M Herman, Jessica M Stephenson, Ting Wu, Ali N Bahadur, Alan R Burns, Sean P Marrelli, Joshua D Wythe
Journal of Neuroscience Research (2019-10-19) <https://doi.org/gr737r>
DOI: [10.1002/jnr.24539](https://doi.org/10.1002/jnr.24539) · PMID: [31630455](https://pubmed.ncbi.nlm.nih.gov/31630455/) · PMCID: [PMC8063604](https://pubmed.ncbi.nlm.nih.gov/PMC8063604/)
21. **3-dimensional visualization of implant-tissue interface with the polyethylene glycol associated solvent system tissue clearing method**
Yating Yi, Yi Men, Dian Jing, Wenjing Luo, Shiwen Zhang, Jian Q Feng, Jin Liu, Woo-Ping Ge, Jun Wang, Hu Zhao
Cell Proliferation (2019-02-03) <https://doi.org/gr7376>
DOI: [10.1111/cpr.12578](https://doi.org/10.1111/cpr.12578) · PMID: [30714253](https://pubmed.ncbi.nlm.nih.gov/30714253/) · PMCID: [PMC6536405](https://pubmed.ncbi.nlm.nih.gov/PMC6536405/)
22. **Multifunctional coatings to simultaneously promote osseointegration and prevent infection of orthopaedic implants**
Jordan Raphel, Mark Holodniy, Stuart B Goodman, Sarah C Heilshorn
Biomaterials (2016-04) <https://doi.org/f8cm8j>
DOI: [10.1016/j.biomaterials.2016.01.016](https://doi.org/10.1016/j.biomaterials.2016.01.016) · PMID: [26851394](https://pubmed.ncbi.nlm.nih.gov/26851394/) · PMCID: [PMC4883578](https://pubmed.ncbi.nlm.nih.gov/PMC4883578/)
23. **Computed tomography: principles, design, artifacts, and recent advances**
Jiang Hsieh
SPIE Optical Engineering Press (2003)
ISBN: 9780819444257
24. **Differential effect of hydroxyapatite nano-particle versus nano-rod decorated titanium micro-surface on osseointegration**
Long Bai, Yanlian Liu, Zhibin Du, Zeming Weng, Wei Yao, Xiangyu Zhang, Xiaobo Huang, Xiaohong Yao, Ross Crawford, Ruiqiang Hang, ... Yin Xiao
Acta Biomaterialia (2018-08) <https://doi.org/gm7sqx>
DOI: [10.1016/j.actbio.2018.06.023](https://doi.org/10.1016/j.actbio.2018.06.023) · PMID: [29908975](https://pubmed.ncbi.nlm.nih.gov/29908975/)
25. **Anti-VEGFs hinder bone healing and implant osseointegration in rat tibiae**
Ahmed Ebraheem Al Subaie, Hazem Eimar, Mohamed-Nur Abdallah, Robert Durand, Jocelyne Feine, Faleh Tamimi, Elham Emami
Journal of Clinical Periodontology (2015-07) <https://doi.org/f7kf9t>
DOI: [10.1111/jcpe.12424](https://doi.org/10.1111/jcpe.12424) · PMID: [26073407](https://pubmed.ncbi.nlm.nih.gov/26073407/)
26. **Neural peptide promotes the angiogenesis and osteogenesis around oral implants**
B Wang, B Wu, Y Jia, Y Jiang, Y Yuan, Y Man, L Xiang
Cellular Signalling (2021-03) <https://doi.org/gr897c>
DOI: [10.1016/j.cellsig.2020.109873](https://doi.org/10.1016/j.cellsig.2020.109873) · PMID: [33285241](https://pubmed.ncbi.nlm.nih.gov/33285241/)

27. **VascuViz: a multimodality and multiscale imaging and visualization pipeline for vascular systems biology**
Akanksha Bhargava, Benjamin Monteagudo, Priyanka Kushwaha, Janaka Senarathna, Yunke Ren, Ryan C Riddle, Manisha Aggarwal, Arvind P Pathak
Nature Methods (2022-02) <https://doi.org/gr897d>
DOI: [10.1038/s41592-021-01363-5](https://doi.org/10.1038/s41592-021-01363-5) · PMID: [35145319](https://pubmed.ncbi.nlm.nih.gov/35145319/) · PMCID: [PMC8842955](https://pubmed.ncbi.nlm.nih.gov/PMC8842955/)
28. **Counteracting age-related VEGF signaling insufficiency promotes healthy aging and extends life span**
M Grunewald, S Kumar, H Sharife, E Volinsky, A Gileles-Hillel, T Licht, A Permyakova, L Hinden, S Azar, Y Friedmann, ... E Keshet
Science (2021-07-30) <https://doi.org/gmc94x>
DOI: [10.1126/science.abc8479](https://doi.org/10.1126/science.abc8479) · PMID: [34326210](https://pubmed.ncbi.nlm.nih.gov/34326210/)
29. **Innovative high-resolution microCT imaging of animal brain vasculature**
Ruslan Hlushchuk, David Haberthür, Petr Soukup, Sébastien Barré, Oleksiy-Zakhar Khoma, Johannes Schittny, Neda Haghayegh Jahromi, Audrey Bouchet, Britta Engelhardt, Valentin Djonov
Brain Structure and Function (2020-10-31) <https://doi.org/gr737t>
DOI: [10.1007/s00429-020-02158-8](https://doi.org/10.1007/s00429-020-02158-8) · PMID: [33128675](https://pubmed.ncbi.nlm.nih.gov/33128675/) · PMCID: [PMC7674347](https://pubmed.ncbi.nlm.nih.gov/PMC7674347/)
30. **Cutting-edge microangio-CT: new dimensions in vascular imaging and kidney morphometry**
Ruslan Hlushchuk, Cédric Zubler, Sébastien Barré, Carlos Correa Shokiche, Laura Schaad, Raphael Röthlisberger, Monika Wnuk, Christoph Daniel, Oleksiy Khoma, Stefan A Tschanz, ... Valentin Djonov
American Journal of Physiology-Renal Physiology (2018-03-01) <https://doi.org/gdbw3b>
DOI: [10.1152/ajpregn.00099.2017](https://doi.org/10.1152/ajpregn.00099.2017) · PMID: [29167169](https://pubmed.ncbi.nlm.nih.gov/29167169/)
31. **Ex vivo microangioCT: Advances in microvascular imaging**
Ruslan Hlushchuk, David Haberthür, Valentin Djonov
Vascular Pharmacology (2019-01) <https://doi.org/ghgd4s>
DOI: [10.1016/j.vph.2018.09.003](https://doi.org/10.1016/j.vph.2018.09.003) · PMID: [30248380](https://pubmed.ncbi.nlm.nih.gov/30248380/)
32. **Correlative Imaging of the Murine Hind Limb Vasculature and Muscle Tissue by MicroCT and Light Microscopy**
Laura Schaad, Ruslan Hlushchuk, Sébastien Barré, Roberto Gianni-Barrera, David Haberthür, Andrea Banfi, Valentin Djonov
Scientific Reports (2017-02-07) <https://doi.org/f9p4pn>
DOI: [10.1038/srep41842](https://doi.org/10.1038/srep41842) · PMID: [28169309](https://pubmed.ncbi.nlm.nih.gov/28169309/) · PMCID: [PMC5294414](https://pubmed.ncbi.nlm.nih.gov/PMC5294414/)
33. **Morphological Aspects of Tumor Angiogenesis**
Ruslan Hlushchuk, Sébastien Barré, Valentin Djonov
Methods in Molecular Biology (2016) <https://doi.org/gr737s>
DOI: [10.1007/978-1-4939-3999-2_2](https://doi.org/10.1007/978-1-4939-3999-2_2) · PMID: [27858352](https://pubmed.ncbi.nlm.nih.gov/27858352/)
34. **Therapeutic Targeting of CD146/MCAM Reduces Bone Metastasis in Prostate Cancer**
Eugenio Zoni, Letizia Astrologo, Charlotte KY Ng, Salvatore Piscuoglio, Janine Melsen, Joël Grosjean, Irena Klima, Lanpeng Chen, Ewa B Snaar-Jagalska, Kenneth Flanagan, ... George N Thalmann
Molecular Cancer Research (2019-05-01) <https://doi.org/gr7379>
DOI: [10.1158/1541-7786.mcr-18-1220](https://doi.org/10.1158/1541-7786.mcr-18-1220) · PMID: [30745464](https://pubmed.ncbi.nlm.nih.gov/30745464/)
35. **Mouse models for studying prostate cancer bone metastasis**
Jinlu Dai, Janine Hensel, Ning Wang, Marianna Kruithof-de Julio, Yusuke Shiozawa

36. **The miniature pig: a useful large animal model for dental and orofacial research**
S Wang, Y Liu, D Fang, S Shi
Oral Diseases (2007-11) <https://doi.org/cs8xz4>
DOI: [10.1111/j.1601-0825.2006.01337.x](https://doi.org/10.1111/j.1601-0825.2006.01337.x) · PMID: [17944668](https://pubmed.ncbi.nlm.nih.gov/17944668/)
37. **Animal models for implant biomaterial research in bone: A review**
AI Pearce, RG Richards, S Milz, E Schneider, SG Pearce
European Cells and Materials (2007-03-02) <https://doi.org/gf9rrt>
DOI: [10.22203/ecm.v013a01](https://doi.org/10.22203/ecm.v013a01) · PMID: [17334975](https://pubmed.ncbi.nlm.nih.gov/17334975/)
38. **Minipig Models of Diabetes Mellitus**
Dwight Bellinger, Elizabeth Merricks, Timothy Nichols
The Minipig in Biomedical Research (2011-12-19) <https://doi.org/fx5bng>
DOI: [10.1201/b11356-37](https://doi.org/10.1201/b11356-37)
39. **Tissue Engineered Neurovascularization Strategies for Craniofacial Tissue Regeneration**
Yiming Li, David Fraser, Jared Mereness, Amy Van Hove, Sayantani Basu, Maureen Newman, Danielle SW Benoit
ACS Applied Bio Materials (2021-11-29) <https://doi.org/gr737z>
DOI: [10.1021/acsabm.1c00979](https://doi.org/10.1021/acsabm.1c00979) · PMID: [35014834](https://pubmed.ncbi.nlm.nih.gov/35014834/) · PMCID: [PMC9016342](https://pubmed.ncbi.nlm.nih.gov/PMC9016342/)
40. **Coupling Osteogenesis and Vasculogenesis in Engineered Orthopedic Tissues**
Nicholas G Schott, Nicole E Friend, Jan P Stegemann
Tissue Engineering Part B: Reviews (2021-06-01) <https://doi.org/gqx6tq>
DOI: [10.1089/ten.teb.2020.0132](https://doi.org/10.1089/ten.teb.2020.0132) · PMID: [32854589](https://pubmed.ncbi.nlm.nih.gov/32854589/) · PMCID: [PMC8349721](https://pubmed.ncbi.nlm.nih.gov/PMC8349721/)
41. **Blood vessel formation and function in bone**
Kishor K Sivaraj, Ralf H Adams
Development (2016-08-01) <https://doi.org/gmgfvb>
DOI: [10.1242/dev.136861](https://doi.org/10.1242/dev.136861) · PMID: [27486231](https://pubmed.ncbi.nlm.nih.gov/27486231/)
42. **Engineering blood vessels and vascularized tissues: technology trends and potential clinical applications**
Prafulla Chandra, Anthony Atala
Clinical Science (2019-05) <https://doi.org/gr7374>
DOI: [10.1042/cs20180155](https://doi.org/10.1042/cs20180155) · PMID: [31088895](https://pubmed.ncbi.nlm.nih.gov/31088895/)
43. **Metastatic bone disease: Pathogenesis and therapeutic options**
Stella D'Oronzo, Robert Coleman, Janet Brown, Francesco Silvestris
Journal of Bone Oncology (2019-04) <https://doi.org/gr737x>
DOI: [10.1016/j.jbo.2018.10.004](https://doi.org/10.1016/j.jbo.2018.10.004) · PMID: [30937279](https://pubmed.ncbi.nlm.nih.gov/30937279/) · PMCID: [PMC6429006](https://pubmed.ncbi.nlm.nih.gov/PMC6429006/)
44. **Impact of Anti-Angiogenic Treatment on Bone Vascularization in a Murine Model of Breast Cancer Bone Metastasis Using Synchrotron Radiation Micro-CT**
Hao Xu, Marie-Hélène Lafage-Proust, Lamia Bouazza, Sandra Geraci, Philippe Clezardin, Bernard Roche, Françoise Peyrin, Max Langer
Cancers (2022-07-15) <https://doi.org/gr738f>
DOI: [10.3390/cancers14143443](https://doi.org/10.3390/cancers14143443) · PMID: [35884504](https://pubmed.ncbi.nlm.nih.gov/35884504/) · PMCID: [PMC9321934](https://pubmed.ncbi.nlm.nih.gov/PMC9321934/)
45. **Open collaborative writing with Manubot**
Daniel S Himmelstein, Vincent Rubinetti, David R Slochower, Dongbo Hu, Venkat S Malladi, Casey S Greene, Anthony Gitter
PLOS Computational Biology (2019-06-24) <https://doi.org/c7np>

